Applied Mathematics and Computation 218 (2012) 10211–10225

Contents lists available at SciVerse ScienceDirect

Applied Mathematics and Computation

journal homepage: www.elsevier.com/locate/amc

Meshless method for solving coupled radiative and conductive heat transfer in complex multi-dimensional geometries

Hamou Sadat *, Cheng-An Wang, Vital Le Dez

Institut PPRIME, CNRS, Université de Poitiers, ENSMA UPR 3346, Département Fluides, Thermique, Combustion, ESIP, Campus Sud 40, avenue du recteur Pineau, 86022 Poitiers Cedex, France

ARTICLE INFO

Keywords:
Meshless method
Coupled radiative–conductive transfer
Discrete ordinates
Even parity
Complex geometries

ABSTRACT

A meshless method DAM is employed to solve the coupled radiative and conductive heat transfer problem in a semi-transparent medium enclosed in complex 2D and 3D geometries. The meshless method for radiative transfer is based on the even parity formulation of the discrete ordinates method. Cases of combined conduction–radiation are presented and the results are compared with other benchmark approximate solutions.

1. Introduction

The coupled problem of conduction and radiation in participating media at high temperature arises in many engineering applications. When the geometry is complex, finite element [2–7] and control volume based finite element methods [8] have been generally employed for the spatial discretization. More recently meshless methods have emerged and have been used successfully in fluid flow [9–17] and related heat transfer problems [18–21]. These methods which do not require the use of a finite element mesh have been also applied in the numerical solution of radiative transfer problems. Liu et al. [22] have proposed a meshless local Petrov–Galerkin (MLPG) approach for solving the coupled radiative and conductive heat transfer in a one-dimensional slab with graded index media. Tan et al. [23] used a least-squares collocation meshless method to solve the coupled radiative and conductive heat transfer in 2D rectangular and cylindrical enclosures. A meshless local Petrov–Galerkin approach with upwind scheme for radiative transfer based on the discrete ordinate equations has been presented in Liu and Tan [24]. Sadat [25] used a moving least squares collocation meshless method with the even parity formulation of the RTE. Another second order method which differs from the even parity formulation was proposed [26] and its comparison with first order formulation was presented in [27]. Like in [25], it was found that the second order approach is more accurate. Wang et al. [28] used the meshless method presented in [25] to solve several purely radiative transfer problems in 2D and 3D geometries. In this paper we extend the method to solve coupled radiative and conductive problems. The details of the theoretical and numerical calculation procedures are given first. Then several 2D and 3D test cases in irregular geometries are considered the results of which are compared with the available literature results.

2. The discrete ordinates method

The discrete ordinates method (DOM) is based on the use of numerical quadratures to approximate the integrals appearing in the calculation of the incident radiation and radiative fluxes. It uses a discretization of the angular space by a finite

* Corresponding author.
E-mail address: hamou.sadat@univ-poitiers.fr (H. Sadat).

0096-3003/$ - see front matter © 2012 Elsevier Inc. All rights reserved.
http://dx.doi.org/10.1016/j.amc.2012.03.101

number of directions along which the RTE is solved. In the primitive variables formulation, considering a discrete ordinate m with coordinate s, for an absorbing, emitting and scattering medium, the RTE writes:

$$\frac{dI(\Omega_m)}{ds} = -\beta I(\Omega_m) + \kappa I_b + \frac{\sigma_s}{4\pi}\sum_{n=1}^{M} I(\Omega'_n)\Phi(\Omega'_n,\Omega_m)W(\Omega'_n), \tag{1}$$

where $m = 1,\ldots,M$ are the discrete ordinates directions, and κ, σ_s and β are the absorption, the scattering and the extinction coefficients, respectively, I_b is the blackbody intensity of the medium, $\Phi(\Omega'_n,\Omega_m)$ is the scattering phase function of intensity entering from Ω'_n scattered to Ω_m and $W(\Omega'_n)$ is the angular weight of ordinate n.

Discrete boundary conditions for diffusely reflecting walls are:

$$I(\Omega_m) = \varepsilon I_{bw} + \frac{1-\varepsilon}{\pi}\sum_{\hat{n}\cdot\Omega'_n<0} I(\Omega'_n)|\hat{n}\cdot\Omega'_n|W(\Omega'_n), \tag{2}$$

where ε is the wall emissivity, I_{bw} is the blackbody intensity of the wall, $\hat{n}$ is the unit inward normal vector at the boundary location and Ω'_n is the unit direction vector of nth ordinate.

Basically, the discrete ordinates (or S_N) method proceeds as follows:

1. The RTE is solved for a discrete set of directions Ω_m, $m = 1,\ldots,M$, leading to the knowledge of $I(\Omega_m)$ in the whole calculation domain for each direction m. In this paper we use a quadrature of S6.
2. Weighting factors $W(\Omega_m)$ are associated to each direction Ω_m whence integration over directions is approximated by the general quadrature formula:

$$\int_{4\pi} I(\Omega)d\Omega = \sum_{m=1}^{M} I(\Omega_m)W(\Omega_m). \tag{3}$$

3. Even-parity formulation of the discrete ordinates method

In the second-order even parity formulation of the RTE, the intensities related to the positive and the negative directions, denoted as $I^+(\Omega)$ and $I^-(\Omega)$, are governed by the two following equations:

$$\frac{dI^+(\Omega)}{ds} = -\beta I^+(\Omega) + \kappa I_b + \frac{\sigma_s}{4\pi}\int_{4\pi} I(\Omega')\Phi(\Omega',\Omega)d\Omega', \tag{4}$$

$$\frac{dI^-(\Omega)}{ds} = \beta I^-(\Omega) - \kappa I_b - \frac{\sigma_s}{4\pi}\int_{4\pi} I(\Omega')\Phi(\Omega',-\Omega)d\Omega'. \tag{5}$$

Introducing the new variables defined as:

$$F(\Omega) = I^+(\Omega) + I^-(\Omega), \tag{6}$$

$$G(\Omega) = I^+(\Omega) - I^-(\Omega), \tag{7}$$

and assuming that the scattering-phase function satisfies the following general condition:

$$\Phi(\Omega',\Omega) = \Phi(-\Omega',-\Omega). \tag{8}$$

It can be shown [29] that one can eliminate one of the variables and write for example for the variable $F(\Omega_m)$ (calculated on each line of sight):

$$\frac{1}{\beta}\frac{dF^2(\Omega_m)}{ds^2} - \beta F(\Omega_m) + 2\kappa I_b + \frac{\sigma_s}{4\pi}\sum_{n=1}^{M/2}(A_{mn}F(\Omega_n) + B_{mn}G(\Omega_n)) = 0, \tag{9}$$

where

$$A_{mn} = \left[\Phi(\Omega'_n,\Omega_m) + \Phi(\Omega'_n,-\Omega_m)\right]W(\Omega'_n) \tag{10}$$

and

$$B_{mn} = \left[\Phi(\Omega'_n,\Omega_m) - \Phi(\Omega'_n,-\Omega_m)\right]W(\Omega'_n). \tag{11}$$

The corresponding boundary condition is:

$$F(\Omega_m) - sign(\hat{n}\cdot\Omega_m)\frac{1}{\beta}\frac{dF(\Omega_m)}{ds} = 2\left(\varepsilon I_{bw} + \frac{1-\varepsilon}{\pi}q'\right), \tag{12}$$

q' being given by:

$$q' = \sum_{n=1}^{M/2}\frac{1}{2}\left[F(\Omega'_n) - sign(\hat{n}\cdot\Omega'_n)G(\Omega'_n)\right]|\hat{n}\cdot\Omega'_n|W(\Omega'_n). \tag{13}$$

Function G can be deduced by using the equation:

$$\frac{dF(\Omega_m)}{ds} = -\beta G(\Omega_m). \tag{14}$$

If we introduce the incident radiation: $H = \int_{4\pi} I(\Omega)d\Omega$ and the net flux on the wall: $q_{r,w} = \int_{4\pi} I(\Omega)(\Omega \cdot \hat{n})d\Omega$, one can show easily that the incident radiation and the net fluxes (in the three Cartesian directions) write respectively:

$$H = \int_{2\pi} F(\Omega)d\Omega = \sum_{m=1}^{M/2} F(\Omega_m)W(\Omega_m), \tag{15}$$

$$q_{r,x} = \int_{2\pi} G(\Omega)(\Omega \cdot \hat{n}_x)d\Omega = \sum_{m=1}^{M/2} G(\Omega_m)(\Omega_m \cdot \hat{n}_x)W(\Omega_m), \tag{16}$$

$$q_{r,y} = \int_{2\pi} G(\Omega)(\Omega \cdot \hat{n}_y)d\Omega = \sum_{m=1}^{M/2} G(\Omega_m)(\Omega_m \cdot \hat{n}_y)W(\Omega_m), \tag{17}$$

$$q_{r,z} = \int_{2\pi} G(\Omega)(\Omega \cdot \hat{n}_z)d\Omega = \sum_{m=1}^{M/2} G(\Omega_m)(\Omega_m \cdot \hat{n}_z)W(\Omega_m). \tag{18}$$

4. Energy equation

The steady state energy conservation equation consisting of both conduction and radiation can be expressed as:

$$k\Delta T - \nabla \cdot \vec{q}_r = 0. \tag{19}$$

For a gray medium of unit refractive index, the divergence of the radiative flux is given by:

$$\nabla \cdot \vec{q}_r = \kappa(4\pi I_b - H), \tag{20}$$

where H is the incident radiation. Substituting Eq. (20) into Eq. (19) yields to the non-dimensional form of energy equation as:

$$\Delta\theta = \frac{1-\omega}{N}\left[\theta^4 - \frac{H^*}{4}\right]. \tag{21}$$

With $\theta = \frac{T}{T_{ref}}$, $N = \frac{k\beta}{4\sigma T_{ref}^3}$, $H^* = \frac{H}{\sigma T_{ref}^4}$ the reduced temperature and non-dimensional numbers.

Here in the above equations, T_{ref} is the reference temperature, N is conduction–radiation parameter and ω is the single scattering albedo $\omega = \frac{\sigma_s}{\beta}$.

The dimensionless heat fluxes Q_x, Q_y, Q_z are the sum of both conduction and radiation components, written as follows:

$$Q_x = \frac{q_x}{\sigma T_{ref}^4} = -4N\frac{\partial\theta}{\beta\partial x} + q_{r,x}, \tag{22}$$

$$Q_y = \frac{q_y}{\sigma T_{ref}^4} = -4N\frac{\partial\theta}{\beta\partial y} + q_{r,y}, \tag{23}$$

$$Q_z = \frac{q_z}{\sigma T_{ref}^4} = -4N\frac{\partial\theta}{\beta\partial z} + q_{r,z}. \tag{24}$$

5. The moving least squares collocation meshless method

The partial differential equations are solved by a moving least squares based meshless method.

Let $\Phi: R^n \to R$ be a scalar field whose values Φ_i are known at the point X_i of a given set of N nodes in the studied domain $D \subset R^n$. The diffuse approximation gives estimates of Φ and its derivatives up to the order k at any point $X \in D$. The Taylor expansion of Φ at X is estimated by a weighted least squares method which uses only the values of Φ at some points X_i situated in the vicinity of X. It can thus be written:

$$\Phi_i^{estimated} = \langle P(X_i - X)\rangle\langle\alpha(X)\rangle^T, \tag{25}$$

where $\langle P(X_i - X)\rangle$ is a colon vector of polynomial basis functions and $\langle\alpha(X)\rangle^T$ is a vector of coefficients which are determined by minimizing the quantity:

$$I(\alpha) = \sum_{i=1}^{N}\omega(X, X_i - X)[\Phi_i - \langle P(X_i - X)\rangle\langle\alpha(X)\rangle^T]^2, \tag{26}$$

in which $\omega(X, X_i - X)$ is a weight-function of compact support, equal to unity at this point, decreasing when the distance to the node increases and zero outside a given domain of influence (a more precise description of $\omega(X, X_i - X)$ will be done next).

Minimization of Eq. (26) then gives:

$$A(X)\alpha(X) = B(X), \tag{27}$$

where

$$A(X) = \sum_{i=1}^{N} \omega(X, X_i - X) P(X_i - X) P^T(X_i - X), \tag{28}$$

$$B(X) = \sum_{i=1}^{N} \omega(X, X_i - X) P(X_i - X) \Phi_i. \tag{29}$$

By inverting system (27), one obtains the components of α which are the derivatives of Φ at X in terms of the neighboring nodal values Φ_i. In this work, the Taylor expansion is truncated at order 2. The polynomial vector used is:

$$\langle P(X_i - X) \rangle = \langle 1, (x_i - x), (y_i - y), (x_i - x)^2, (x_i - x) \cdot (y_i - y), (y_i - y)^2 \rangle \tag{30}$$

and we have:

$$\langle \alpha_1, \alpha_2, \alpha_3, \alpha_4, \alpha_5, \alpha_6 \rangle^T = \left\langle \Phi, \frac{\partial \Phi}{\partial x}, \frac{\partial \Phi}{\partial y}, \frac{\partial^2 \Phi}{2\partial x^2}, \frac{\partial \Phi^2}{\partial x \partial y}, \frac{\partial^2 \Phi}{2\partial y^2} \right\rangle^T. \tag{31}$$

Finally, the following system is obtained:

$$\begin{Bmatrix} \varphi \\ \frac{\partial \varphi}{\partial x} \\ \frac{\partial \varphi}{\partial y} \\ \frac{\partial^2 \varphi}{2!\partial x^2} \\ \frac{\partial^2 \varphi}{\partial x \partial y} \\ \frac{\partial^2 \varphi}{2!\partial y^2} \end{Bmatrix}^* = [A(X)]^{-1} \cdot \left\{ \sum_{i=1}^{n'(X)} \omega(X, X_i - X) \cdot \langle P(X_i - X) \rangle^T \cdot \Phi_i \right\}. \tag{32}$$

The square matrix $A(X)$ is not singular as long as the number $n'(X)$ of the connected nodes at a given point is at least equal to the size of $\langle P(X_i - X) \rangle$ and are not all situated in the same plane (in 3D) or line (in 2D).

In our studies, several weight-functions were tried and it was found that the following Gaussian window:

$$\omega(M_j, M) = \exp\left[-3\ln(10) \cdot \left(\frac{r}{\sigma_{\inf}} \right)^2 \right], \tag{33}$$

$$\omega(M_j, M) = 0, \quad \text{if } r > \sigma_{\inf} \tag{34}$$

behaves rather well. The distance of influence $\sigma_{\inf}$ is updated at each point.

The previous approximation is then used in a point collocation method to solve partial derivatives equations. At each point of the discretization, the derivatives appearing in the equation to be solved are replaced by their diffuse approximation thus leading to an algebraic system that is solved after the introduction of the boundary conditions. The Dirichlet type boundary conditions are introduced in the same way as in the finite element method. The Neumann boundary conditions on the other hand are replaced by their diffuse approximation and then introduced in the algebraic system.

6. Discretization schemes

In this section, we write the discretization schemes obtained by the collocation meshless method for the RTE and the energy equation which are solved on the same set of nodes. In the following, we set $\langle p(M_j, M) \rangle = \langle p_j \rangle$ and we define $\langle a_i \rangle$ as the ith line of the inverse matrix $[A^M]^{-1}$.

6.1. Two dimensional problems

For 2D problems, the even parity formulation Eq. (9) can be written as:

$$\frac{1}{\beta} \left(\mu_m^2 \frac{\partial^2 F(\Omega_m)}{\partial x^2} + \eta_m^2 \frac{\partial^2 F(\Omega_m)}{\partial y^2} + 2\mu_m \eta_m \frac{\partial^2 F(\Omega_m)}{\partial x \partial y} \right) - \beta F(\Omega_m) + 2\kappa I_b + \frac{\sigma_s}{4\pi} \sum_{n=1}^{M/2} (A_{mn} F(\Omega_n) + B_{mn} G(\Omega_n)) = 0, \tag{35}$$

where μ_m and η_m are the cosine directors of the line of sight m.

By using the explicit relations of the derivatives given by Eq. (32), at each point of the calculation grid, one obtains the following algebraic systems for the radiative (RAD) and conductive (COND) equations respectively:

$$[\text{RAD}] \cdot [F_i] = [S_R], \tag{36}$$

$$[\text{COND}] \cdot [\theta_i] = [S_C], \tag{37}$$

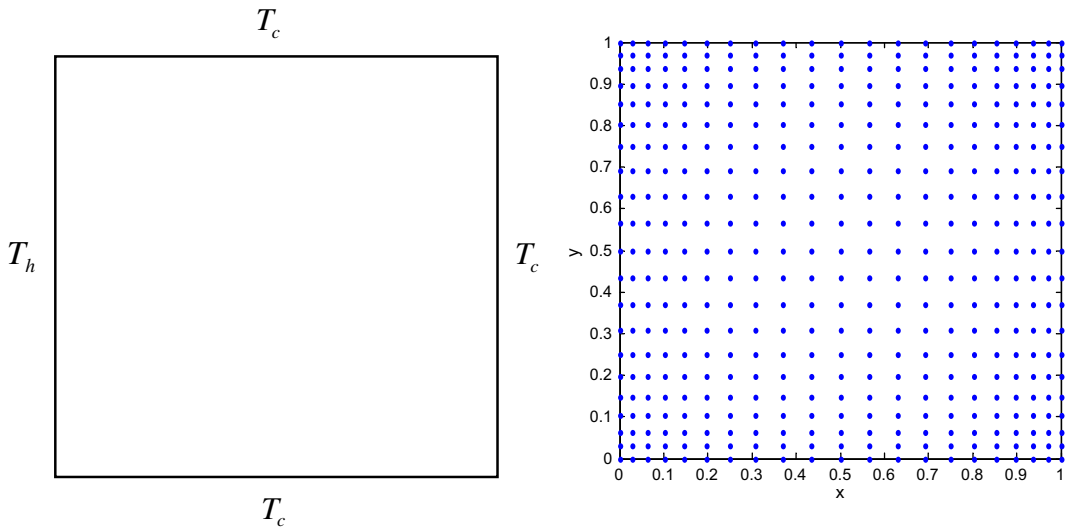

Fig. 1. Square enclosure and distribution of nodes.

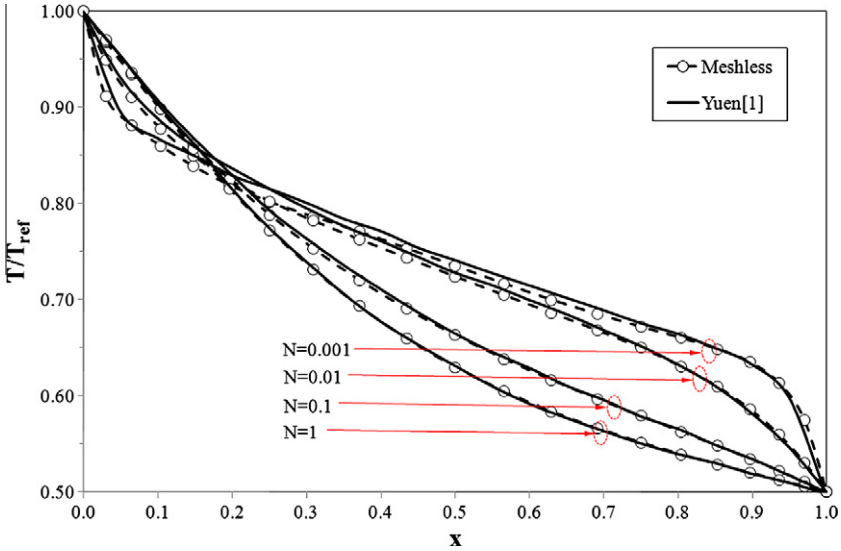

Fig. 2. Dimensionless temperature profiles for various conduction to radiation parameters N along symmetry line.

where we have:

$$\mathrm{RAD}(i,j) = \omega(M_j, M) \cdot \left[\frac{1}{\beta}\left(\mu_m^2 2!\langle a_4\rangle + \eta_m^2 2!\langle a_6\rangle + 2\mu_m\eta_m\langle a_5\rangle\right)\right] \cdot \langle p_j\rangle^T - \beta \cdot \delta_{ij}, \tag{38}$$

where δ_{ij} is Kronecker symbol.

$$\mathrm{COND}(i,j) = \omega(M_j, M) \cdot [2!(\langle a_4\rangle + \langle a_6\rangle)] \cdot \langle p_j\rangle^T \tag{39}$$

and

$$S_R(i) = -\left(2\kappa I_b(i) + \frac{\sigma_s}{4\pi}\sum_{n=1}^{M/2}(A_{mn}F(\Omega_n) + B_{mn}G(\Omega_n))\right), \tag{40}$$

$$S_C(i) = \frac{1-\omega}{N}\left[\theta^4(i) - \frac{H^*}{4}\right]. \tag{41}$$

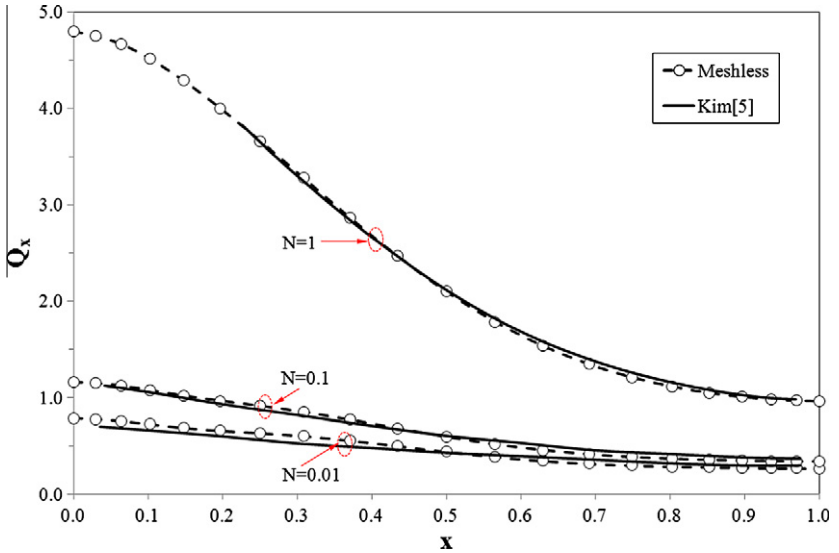

Fig. 3. Dimensionless heat flux profiles for various conduction to radiation parameters N along the symmetry line.

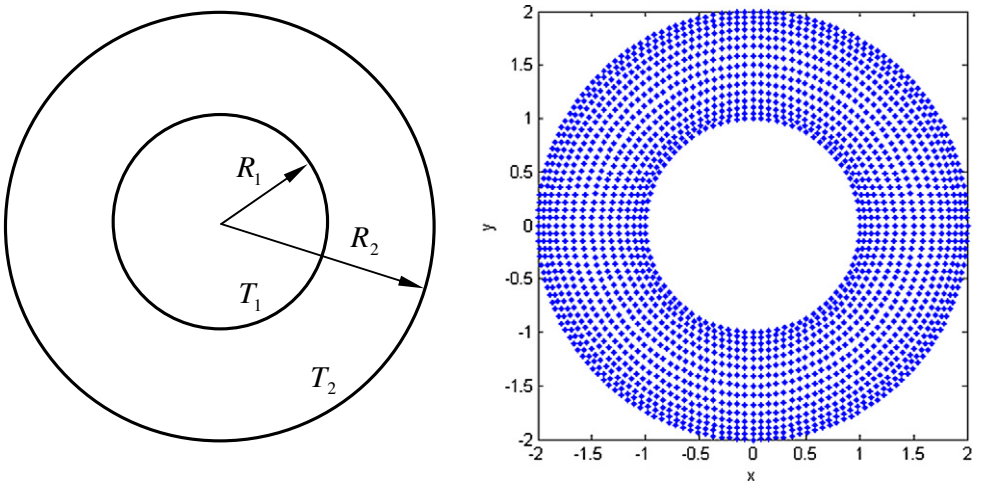

Fig. 4. Cylindrical ring enclosure and the distribution of nodes.

6.2. Three dimensional problems

For 3D problems, the governing equation (9) is written as:

$$\frac{1}{\beta}\left(\begin{array}{l}\mu_m^2\frac{\partial^2 F(\Omega_m)}{\partial x^2}+\eta_m^2\frac{\partial^2 F(\Omega_m)}{\partial y^2}+\xi_m^2\frac{\partial^2 F(\Omega_m)}{\partial z^2}+2\mu_m\eta_m\frac{\partial^2 F(\Omega_m)}{\partial x\partial y}\\ +2\mu_m\xi_m\frac{\partial^2 F(\Omega_m)}{\partial x\partial z}+2\eta_m\xi_m\frac{\partial^2 F(\Omega_m)}{\partial y\partial z}\end{array}\right)-\beta F(\Omega_m)+2\kappa I_b+\frac{\sigma_s}{4\pi}\sum_{n=1}^{M/2}(A_{mn}F(\Omega_n)+B_{mn}G(\Omega_n))=0, \tag{42}$$

where μ_m, η_m, ξ_m are now the three components of the unit direction vector.

In this case, the coefficients of the systems matrices are written as:

$$\mathrm{RAD}(i,j)=\omega(M_j,M)\cdot\left[\frac{1}{\beta}\left(\begin{array}{l}\mu_m^2 2!\langle a_4\rangle+\eta_m^2 2!\langle a_6\rangle+\xi_m^2 2!\langle a_{10}\rangle+2\mu_m\eta_m\langle a_5\rangle\\ +2\mu_m\xi_m\langle a_8\rangle+2\eta_m\xi_m\langle a_9\rangle\end{array}\right)\right]\cdot\langle p_j\rangle^T-\beta\cdot\delta_{ij}, \tag{43}$$

$$\mathrm{COND}(i,j)=\omega(M_j,M)\cdot[2!(\langle a_4\rangle+\langle a_6\rangle+\langle a_{10}\rangle)]\cdot\langle p_j\rangle^T, \tag{44}$$

$$S_R(i)=-\left(2\kappa I_b(i)+\frac{\sigma_s}{4\pi}\sum_{n=1}^{M/2}(A_{mn}F(\Omega_n)+B_{mn}G(\Omega_n))\right), \tag{45}$$

$$S_C(i)=\frac{1-\omega}{N}\left[\theta^4(i)-\frac{H^*}{4}\right]. \tag{46}$$

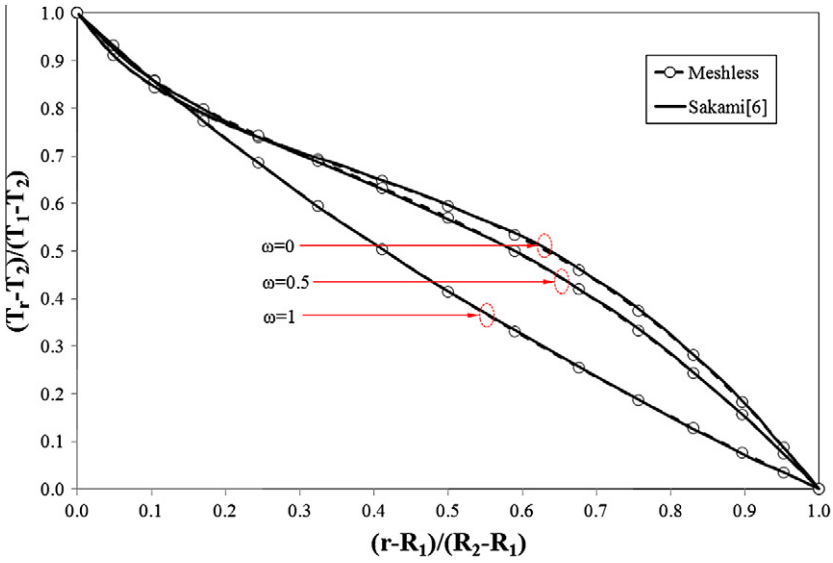

Fig. 5. Dimensionless temperature distribution along radius axis with different albedo.

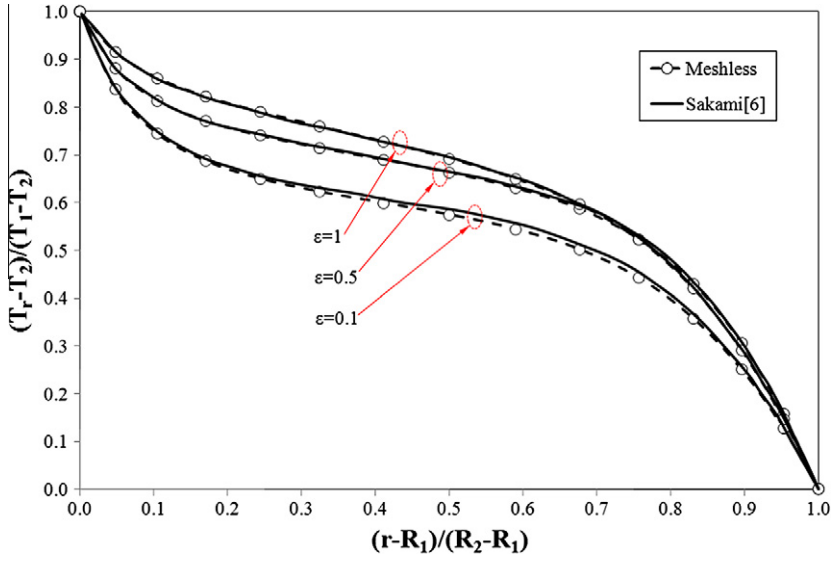

Fig. 6. Dimensionless temperature distribution along radius axis with different emissivity.

6.3. Boundary conditions

For the points lying in the boundary, Eq. (12) leads to:

$$\mathrm{RAD}(i,j) = \omega(M_j,M)\cdot\left[-sign(\hat{n}\cdot\Omega_m)\frac{1}{\beta}(\mu_m\langle a_2\rangle+\eta_m\langle a_3\rangle)\right]\cdot\langle p_j\rangle^T+\delta_{ij}, \tag{47}$$

$$\mathrm{RAD}(i,j) = \omega(M_j,M)\cdot\left[-sign(\hat{n}\cdot\Omega_m)\frac{1}{\beta}(\mu_m\langle a_2\rangle+\eta_m\langle a_3\rangle+\xi_m\langle a_7\rangle)\right]\cdot\langle p_j\rangle^T+\delta_{ij}. \tag{48}$$

For the 2D and 3D problems respectively while the source term writes:

$$S_R(i) = 2\left(\varepsilon I_{bw}(i)+\frac{1-\varepsilon}{\pi}q'\right). \tag{49}$$

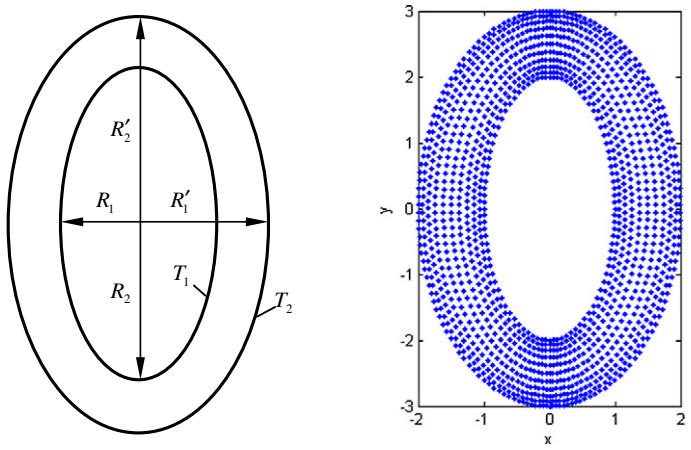

Fig. 7. Elliptical ring enclosure and the distribution of nodes.

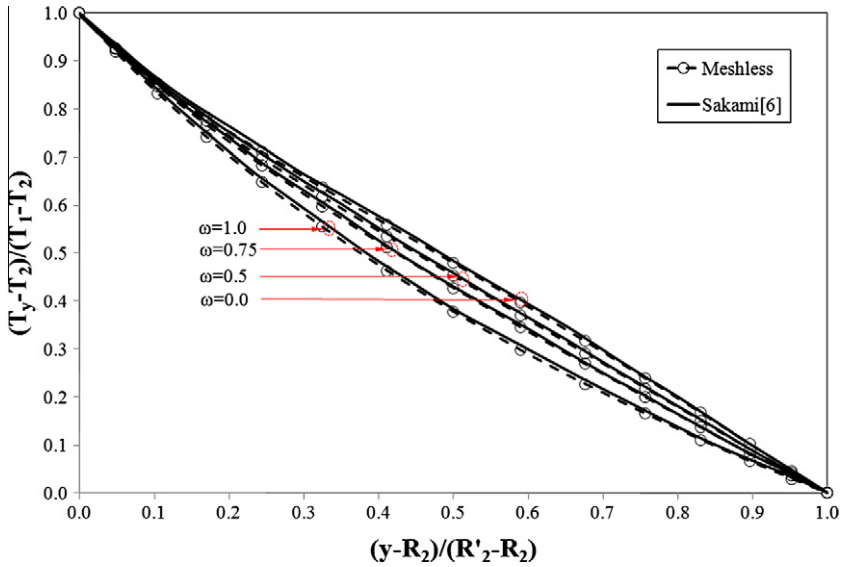

Fig. 8. Dimensionless temperature profiles for various scattering albedo along the symmetry line ($N = 0.1$).

Dirichlet boundary conditions for the energy equation are introduced in the same way as in the finite element approach by using the method of the unity term in the diagonal of the corresponding system matrix.

6.3.1. Iterative process

Obviously the coupled systems are highly non linear. We have therefore chosen the following iterative process to solve them.

1. Choose a finite number of nodes in the domain and on the boundaries. Use DAM method to calculate the derivatives of all the points.
2. Initial temperature field is guessed.
3. Solve the radiative problem.
4. Solve the energy equation.
5. Terminate the iteration process if the convergence criterion is satisfied. Otherwise, go back to step 3.

The convergence criterion used for the numerical calculation is defined as following:

$$\left|\frac{T_{new}-T_{old}}{T_{new}}\right|_{\max} \leqslant 10^{-5}.$$

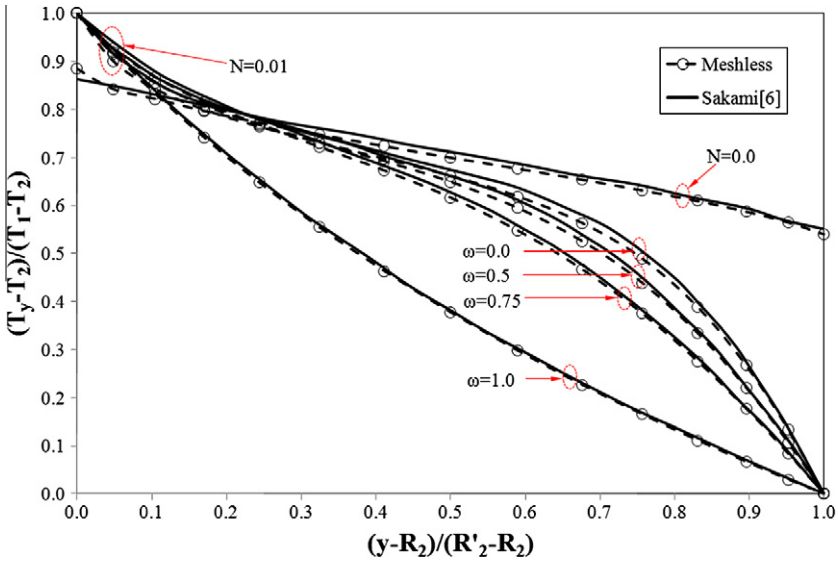

Fig. 9. Dimensionless temperature profiles for various scattering albedo along the symmetry line ($N = 0.01$ and $N = 0.0$).

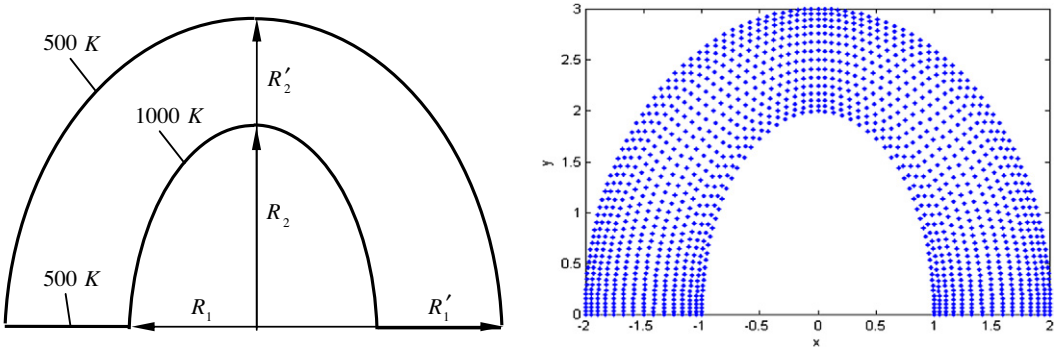

Fig. 10. Half elliptical ring enclosure and the distribution of nodes.

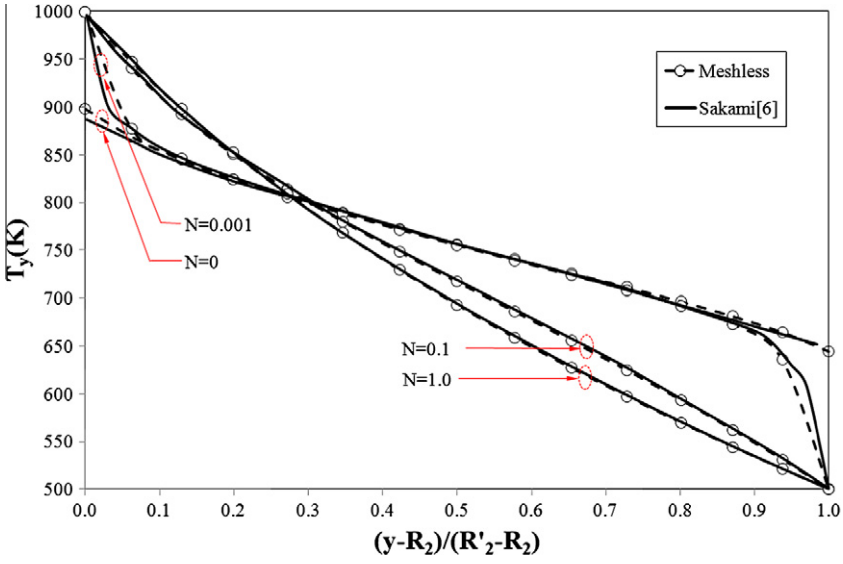

Fig. 11. Effect of conduction to radiation parameter N on temperature profiles along the symmetry ($\beta = 1.0\ m^{-1}$).

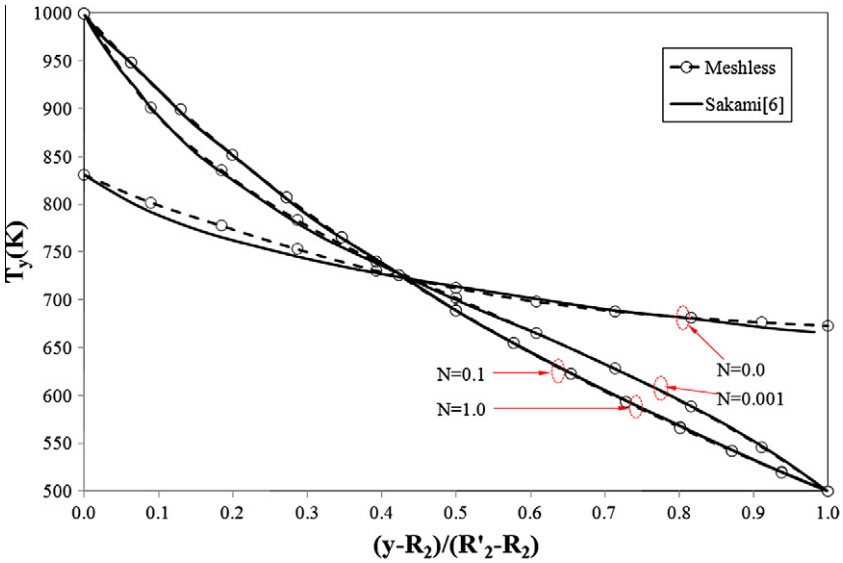

Fig. 12. Effect of conduction to radiation parameter N on temperature profiles along the symmetry ($\beta = 0.1\ m^{-1}$).

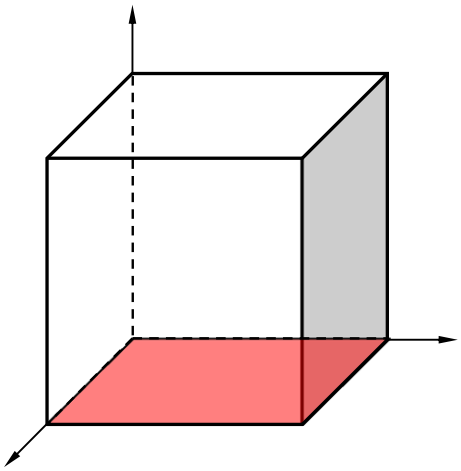

Fig. 13. Cubic geometry and boundary conditions.

7. Two-dimensional results

This section is devoted to the results obtained on some two-dimensional problems.

7.1. Two-dimensional square enclosure

We first consider a square containing a gray absorbing–emitting medium in radiative–conductive equilibrium (Fig. 1). The walls are black; the left one is at a high temperature T_{hot} and the other three walls are at temperature T_{cold}, such that $T_{cold}/T_{hot} = 0.5$. A non uniform 21×21 grid is used and the absorption coefficient is set to $\kappa = 1.0\ m^{-1}$.

The dimensionless temperature profiles and heat flux profiles along the symmetry line at $y = 0.5$ are shown in Figs. 2 and 3 and compared with the results of Refs. [1,5] respectively. The above results show that the meshless method has a good agreement with the reference solution in this test case.

7.2. Cylindrical ring enclosure

Consider now an absorbing–emitting–scattering medium in a 2D cylindrical ring, with radii R_1 and R_2, shown in Fig. 4. The ratio of internal temperature T_1 to external temperature T_2 is $T_1/T_2 = 10$. Let β and ω be the extinction and scattering albedo

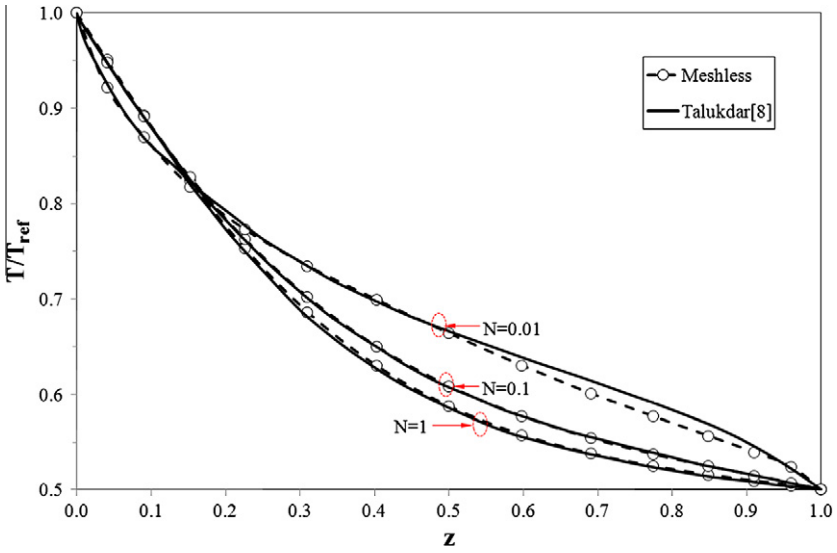

Fig. 14. Effect of conduction to radiation parameter N on centerline temperature along z-direction at $y = 0.5$ and $x = 0.5$ of the cubical enclosure.

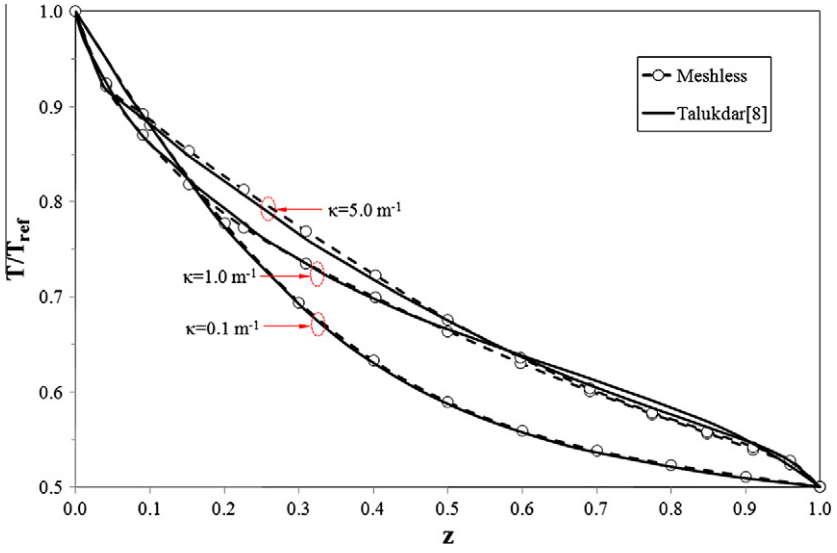

Fig. 15. Effect of κ on centerline temperature along z-direction at $y = 0.5$ and $x = 0.5$ of the cubical enclosure.

coefficients respectively. We present in Fig. 5, the radial a dimensional temperature for a wall emissivity $\varepsilon = 0.5$, a coupled parameter $N = 0.03$ and for different values of the albedo, namely $(\omega = 1.0, 0.5, 0)$. The results are in very good agreement with the results of [6] who used discrete ordinate method. Then the influence of the boundary wall emissivity $(\varepsilon = 0.1, 0.5, 1.0)$ is analyzed for a scattering albedo $\omega = 0$ and a coupled parameter$N = 0.01$. The results presented on Fig. 6 together with those of [6] show good agreement once again.

7.3. Elliptical ring enclosure

The enclosure has now an elliptical shape and the walls are all black Fig. 7. The medium is absorbing, emitting and scattering with an extinction coefficient β. The inner and outer half-axis are such that the optical thicknesses are $\beta R_1 = 1$, $\beta R_1' = 2$, $\beta R_2 = 2$ and $\beta R_2' = 3$, respectively. The ratio of interior elliptical temperature T_1 to exterior elliptical temperature T_2 is $T_1/T_2 = 10$.

The influence of the scattering albedo is first analyzed for different coupled parameter $(N = 0.1, 0.01, 0)$ in Figs. 8 and 9. When the Planck number becomes lower, the effect of the albedo becomes significant. For all cases $(N > 0)$, the temperature results at $\omega = 1$ are identical since radiation transfer is then independent from the energy equation. At radiative equilibrium $(N = 0)$, the effect of the albedo disappears completely. All the results agree very well with those of Ref. [6].

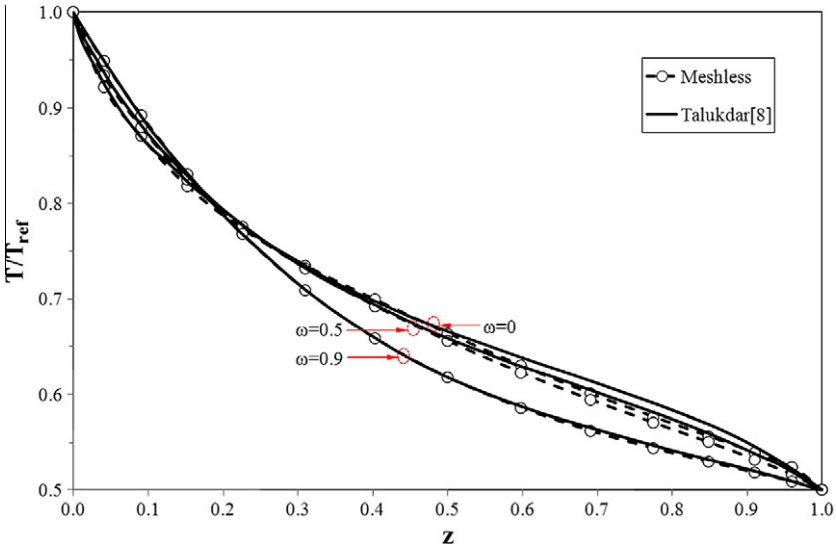

Fig. 16. Effect of ω on centerline temperature along z-direction at $y = 0.5$ and $x = 0.5$ of the cubical enclosure.

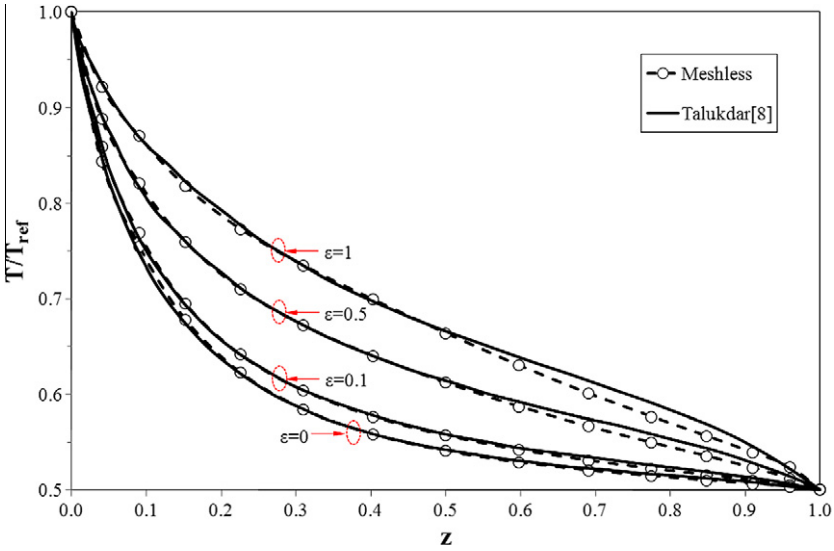

Fig. 17. Effect of ε on centerline temperature along z-direction at $y = 0.5$ and $x = 0.5$ of the cubical enclosure.

7.4. Half elliptical ring enclosure

The internal face is maintained at 1000 K and the other faces at 500 K. The medium is absorbing–emitting and radiative–conductive. The inner and outer half-axis are such that the optical thicknesses are $\beta R_1 = 1$, $\beta R_1' = 2$, $\beta R_2 = 2$ and $\beta R_2' = 3$, respectively (see Fig. 10). The dimensionless temperature profiles along the symmetry are shown in Figs. 11 and 12, for different N at different optical thicknesses. Once more, as it can be seen, the discrepancy of the results between this work and [6] is very small for all values of N and both optical thicknesses β.

8. Three-dimensional results

It has been seen from extensive literature that seldom people work on the 3D conduction–radiation interaction for complex geometries. Here we only consider the cases of cubic and cylindrical enclosures and compare our results with those of [8] (see Fig. 13).

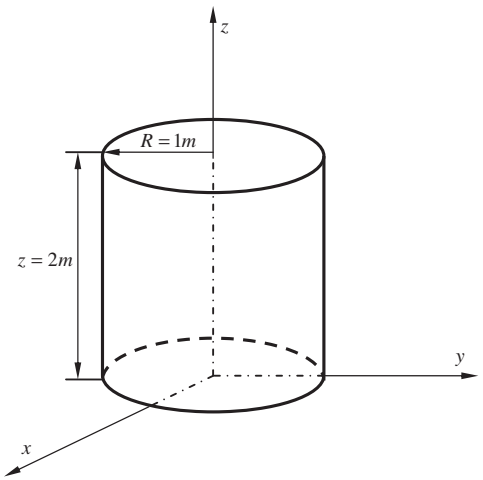

Fig. 18. Cylindrical enclosure.

8.1. Cubic enclosure

We consider a cubic enclosure containing a gray absorbing–emitting–scattering medium in radiative–conductive equilibrium. The bottom wall is at a high temperature T_{hot} and other walls are at T_{cold}, such that $T_{cold}/T_{hot} = 0.5$. Temperature results along z direction at $x = 0.5$ and $y = 0.5$ are presented in Figs. 14–17. A 15^3 nodal discretization is used for all the cases except for $\beta = 0.1\ m^{-1}$ where a 11^3 discretization was used.

We present in Fig. 14 the temperature profile for different values of N in the case of a non scattering media ($\omega = 0$) enclosed in black boundaries with $\beta = 1.0\ m^{-1}$. One can see that there is a good agreement with the results of [8]. The effect of the absorption coefficient κ is shown in Fig. 15 for $N = 0.01$ and black boundaries. The effect of scattering albedo ω has then been considered for $\beta = 1.0\ m^{-1}$, $N = 0.01$ and the results are shown in Fig. 16. One can see that scattering has a little influence on over the medium temperature. On the other hand, medium temperature near the cold boundary increases for a non scattering ($\omega = 0$). The influence of hot boundary emissivity ε has finally been considered for $\beta = 1.0\ m^{-1}$, $\omega = 0$ and $N = 0.01$. Fig. 17 shows the temperature profiles obtained for different emissivities. As expected, the medium temperature increases more and more as the hot boundary emissivity increases. In all studied cases it is seen that the meshless method gives similar results as the finite volume method. It is worth noting here that for the finest grid, the maximum number of iterations

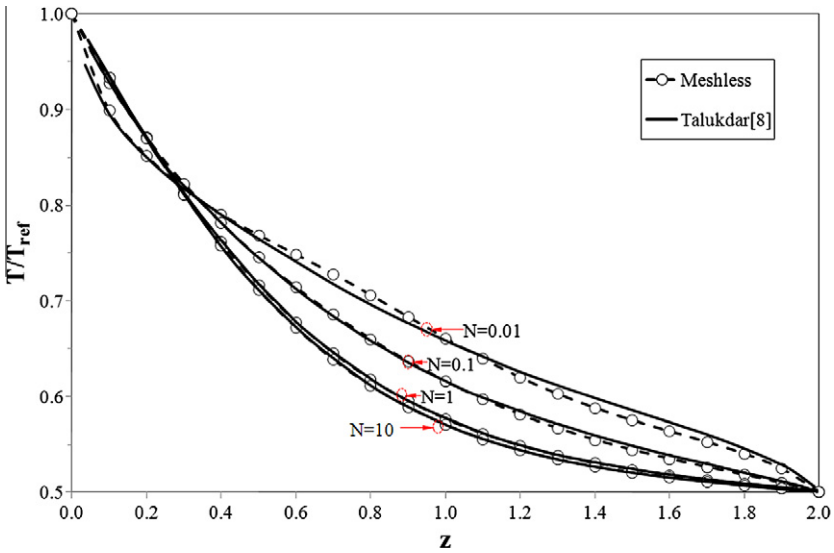

Fig. 19. Effect of conduction to radiation parameter N on centerline temperature along z-direction at $y = 0$ and $x = 0$ of the cylindrical enclosure.

necessary for convergence and CPU time were equal to 75 and 84 min respectively. All the calculations have been done on a PC (3 GHz and 3.25 Go RAM). These values were found equal to 73 and 34 s for the two dimensional square enclosure.

8.2. Cylindrical enclosure

In this last example, we consider a cylindrical enclosure of radius $R = 1$ m and height $z = 2$ m (Fig. 18) filled with a participating medium.

The bottom boundary at $z = 0$ is kept at temperature T_{hot} and other walls are maintained at T_{cold}, such that $T_{cold}/T_{hot} = 0.5$. The temperature distribution along the centerline z at $x = 0$ and $y = 0$ is shown in Fig. 19 for different N. The results are in excellent agreement with the literature results [8].

9. Conclusion

A diffuse approximation meshless method (DAM) is employed for solving radiative–conductive transfer in 2D and 3D complex geometries. The results are compared with other benchmarks results and a good agreement has been observed. The results show that diffuse approximation method has a good accuracy in solving radiative–conductive heat transfer in absorbing, emitting and scattering media in complex geometries. Coupled convection–radiation problems can be solved by a similar approach.

References

[1] W.W. Yuen, E.E. Takara, Analysis of combined conductive–radiative heat transfer in a two-dimensional rectangular enclosure with a gray medium, J. Heat Transfer 110 (1988) 468–474.
[2] M.L. Nice, Applications of finite elements to heat transfer in a participating medium, in: T.M. Shih (Ed.), Numerical Properties and Methodologies in Heat Transfer, Hemisphere, Washington, DC, 1983, pp. 497–514.
[3] M.M. Razzaque, J.R. Howell, D.E. Klein, Coupled radiative and conductive heat transfer in a two-dimensional rectangular enclosure with gray participating media using finite elements, J. Heat Transfer 106 (1984) 613–619.
[4] S.P. Burns, J.R. Howell, D.E. Klien, Empirical evaluation of an important approximation for combined-mode heat transfer in a participating medium using the finite element method, Numer. Heat Transfer, Part B 27 (1995) 309–322.
[5] T.Y. Kim, S.W. Baek, Analysis of combined conductive and radiative heat transfer in a two-dimensional rectangular enclosure using the discrete ordinates method, Int. J. Heat Mass Transfer 34 (1991) 2265–2273.
[6] M. Sakami, A. Charette, V. Le Dez, Application of the discrete ordinates method to combined conductive and radiative heat transfer in a two-dimensional complex geometry, J. Quant. Spectrosc. Radiat. Transfer 56 (4) (1996) 517–533.
[7] L.M. Ruan, M. Xie, H. Qi, W. An, H.P. Tan, Development of a finite element model for coupled radiative and conductive heat transfer in participating media, J. Quant. Spectrosc. Radiat. Transfer 102 (2) (2006) 190–202.
[8] P. Talukdar, F.V. Issendorff, D. Trimis, C.J. Simonson, Conduction–radiation interaction in 3D irregular enclosures using the finite volume method, Heat Mass Transfer 44 (2008) 695–704.
[9] C. Prax, H. Sadat, Collocated diffuse approximation for channel flows, Mech. Res. Commun. 23 (1) (1996) 61–66.
[10] C. Prax, H. Sadat, Application of the diffuse approximation for solving fluid flow and heat transfer problems, Int. J. Heat Mass Transfer 39 (1) (1996) 214–218.
[11] S. Couturier, H. Sadat, Résolution des équations de Navier–Stokes dans la formulation en variables primitives par approximation diffuse, Comptes Rend. Acad. Sci., t. 326, série II b, (1998) 117–119.
[12] C. Prax, H. Sadat, E. Dabboura, Evaluation of high order versions of the diffuse approximate meshless method, Appl. Math. Comput. 186 (2) (2007) 1040–1053.
[13] H. Sadat, S. Couturier, Performance and accuracy of a meshless method for laminar natural convection, Numer. Heat Transfer, Part B: Fundam. 37 (4) (2000) 455–467.
[14] C. Prax, P. Salagnac, H. Sadat, Diffuse approximation and control-volume-based finite-element methods: a comparative study, Numer. Heat Transfer, Part B: Fundam. 34 (3) (1998) 303–321.
[15] T. Sophy, H. Sadat, C. Prax, A meshless formulation for three dimensional laminar natural convection, Numer. Heat Transfer, Part B: Fundam. 41 (5) (2002) 433–445.
[16] Yunxin Zhang, Convergence of meshless Petrov–Galerkin method using radial basis functions, Appl. Math. Comput. 183 (1) (2006) 307–321.
[17] C. Prax, H. Sadat, P. Salagnac, Diffuse approximation method for solving natural convection in porous media, Transp. Porous Media 22 (2) (1996) 215–223.
[18] Xinghui Cai, G.H. Su, Suizheng Qiu, Local radial point interpolation method for the fully developed magnetohydrodynamic flow, Appl. Math. Comput. 217 (9) (2011) 4529–4539.
[19] O. Bertrand, B. Binet, H. Combeau, S. Couturier, Y. Delannoy, D. Gobin, M. Lacroix, P. Le Quere, M. Medale, J. Mencinger, H. Sadat, G. Vieira, Melting driven by natural convection A comparison exercise: first results, Int. J. Therm. Sci. 38 (1) (1999) 5–26.
[20] H. Sadat, N. Dubus, L. Gbahoué, T. Sophy, On the solution of heterogeneous heat conduction problems by a diffuse approximation meshless method, Numer. Heat Transfer, Part B: Fundam. 50 (6) (2006) 491–498.
[21] K.B. Cheong, T.H. Song, Examination of solution methods for the second-order discrete ordinate formulation, Numer. Heat Transfer B 27 (1995) 155–173.
[22] L.H. Liu, J.Y. Tan, B.X. Li, Meshless approach for coupled radiative and conductive heat transfer in one-dimensional graded index medium, J. Quant. Spectr. Radiat. Transfer 101 (2006) 237–248.
[23] J.Y. Tan, L.H. Liu, B.X. Li, Least-squares collocation meshless approach for coupled radiative and conductive heat transfer, Numer. Heat Transfer, Part B: Fundam. 49 (2) (2006) 179–195.
[24] L.H. Liu, J.Y. Tan, Meshless local Petrov–Galerkin approach for coupled radiative and conductive heat transfer, Int. J. Therm. Sci. 46 (2007) 672–681.
[25] H. Sadat, On the use of a meshless method for solving radiative transfer with the discrete ordinates formulation, J. Quant. Spectr. Radiat. Transfer 101 (2) (2006) 263–268.
[26] J.M. Zhao, L.H. Liu, Second-order radiative transfer equation and its properties of numerical solution using the finite-element method, Numer. Heat Transfer, Part B 51 (2007) 391–409.

[27] J.Y. Tan, J.M. Zhao, L.H. Liu, Y.Y. Wang, Comparative study on accuracy and solution cost of the first/second-order radiative transfer equations using the meshless method, Numer. Heat Transfer, Part B 55 (2009) 324–337.
[28] C.A. Wang, H. Sadat, V. Le dez, D. Lemonnier, Meshless method for solving radiative transfer problems in complex two-dimensional and three-dimensional geometries, Int. J. Therm. Sci. 49 (2010) 2282–2288.
[29] K.B. Cheong, T.H. Song, Examination of solution methods for the second-order discrete ordinate formulation, Numer. Heat Transfer B 27 (1995) 155–173.